

## ABSTRACT

Title of Thesis: CHARACTERIZATION OF ELECTRODEPOSITED  
CHITOSAN FILMS BY ATOMIC FORCE  
MICROSCOPY AND RAMAN SPECTROSCOPY

Erin C. Dreyer, Master of Science, 2006

Thesis Directed By: Professor Gary W. Rubloff  
Department of Materials Science and Engineering

Chitosan has served as a robust and reproducible scaffold for biological reactions by electrodeposition at specific sites in microfluidic channels. However, its growth and properties are not well understood as a function of deposition parameters. To better understand the materials and process science, in-vitro characterization techniques and post-deposition measurements of air-dried films were performed. AFM images of dried films depicted variable, rough morphology not directly correlated to deposition conditions while hydration increased surface homogeneity. Dry roughness increased logarithmically with thickness supporting growth by nucleation. In-vitro fluorescence images showed fairly smooth distribution of chitosan, whereas dried films were much rougher, indicating non-uniform collapse of structure during drying. Raman spectroscopy revealed the presence of primary amine groups active in biofunctionalization and served as a technique for evaluating the spatial selectivity of chitosan by electrodeposition. Further study of hydrated films is needed to fully understand chitosan as a platform for biotechnology applications.

CHARACTERIZATION OF ELECTRODEPOSITED CHITOSAN FILMS BY  
ATOMIC FORCE MICROSCOPY AND RAMAN SPECTROSCOPY

by

Erin C. Dreyer

Thesis submitted to the Faculty of the Graduate School of the  
University of Maryland, College Park, in partial fulfillment  
of the requirements for the degree of  
Masters of Science  
2006

Advisory Committee:

Professor Gary Rubloff, Chair  
Professor Mohamad Al-Sheikhly  
Professor Isabel Lloyd

© Copyright by

Erin C. Dreyer

2006

## ACKNOWLEDGEMENTS

Finishing a B.S. and M.S. in engineering in five years is no easy task. During the past year and a half of research, many people supported me throughout the good and bad times. First I would like to thank Dr. Rubloff's entire bioMEMS group for their help and input at meetings and in the lab. I would especially like to thank Jung Jin Park and Susan Beatty who both took me under their wings and taught me the ins and outs of chitosan deposition. Jin and Susan performed the first chitosan deposition, giving me more responsibility with each successive deposition. What once seemed so complicated became so familiar. Thanks to Jin for always being around to help me troubleshoot, and to Susan and Jin for measuring the dry thicknesses via profilometry. Many thanks also go out to Dr. Michael Dreyer who trained me so well on the AFM at LPS. I would also like to thank Dr. Vince Ballarotto, Sergey Mezheny, and Mihaela Breban for training me on the Raman microscope at LPS.

A well-deserved thank you also goes out to Dr. Kathleen Hart who has been an amazing friend and a very knowledgeable coordinator. Thank you to Prof. Isabel Lloyd for giving me so much more than my first research position; she gave me the confidence I needed to excel and introduced me to the five-year program. Most importantly I would like to thank my advisor Prof. Gary Rubloff for intellectual, financial, and emotional support, for the great amount of flexibility and freedom, and for understanding. Thank you for all your help and guidance and for having faith in me.

## TABLE OF CONTENTS

ACKNOWLEDGEMENTS .....	ii
TABLE OF CONTENTS.....	iii
LIST OF FIGURES .....	vi
LIST OF TABLES .....	v
LIST OF ACRONYMS AND ABBREVIATIONS .....	vii
Chapter 1: Introduction .....	1
1.1 Chitosan .....	2
1.2 Previous Work .....	3
1.3 Motivation.....	5
Chapter 2: Experimental .....	6
2.1 Chitosan Deposition.....	6
2.1.1 <i>Making Chitosan Solution</i> .....	7
2.1.2 <i>Chitosan Deposition</i> .....	9
2.2 Film Characterization.....	11
2.2.1 <i>Film Thickness</i> .....	11
2.2.2 <i>Atomic Force Microscopy</i> .....	11
2.2.3 <i>Raman Spectroscopy</i> .....	14
2.3 Hypotheses.....	14
2.4 Experimental Parameters .....	15
2.4.1 <i>Deposition A: 02/08/05</i> .....	16
2.4.2 <i>Deposition B: 04/13/05</i> .....	16
2.4.3 <i>Deposition C: 05/12/05</i> .....	17
2.4.4 <i>Deposition D: 08/17/05</i> .....	17
2.4.5 <i>Deposition E: 11/16/05</i> .....	18
2.4.6 <i>Deposition F: 02/09/06</i> .....	19
Chapter 3: Thickness vs. Time and Current Density .....	20
3.1 Deposition A .....	20
3.2 Deposition B .....	21
3.3 Deposition C .....	22
3.4 Deposition D .....	23
3.5 Deposition E.....	24
Chapter 4: Roughness vs. Thickness .....	26
4.1 The Effect of Scan Size.....	26
4.2 Deposition A.....	27
4.3 Deposition B .....	30

4.4 Deposition C .....	31
4.5 Deposition E.....	32
4.6 Discussion.....	34
4.6.1 <i>Deposition Error</i> .....	35
4.6.2 <i>Measurement and Analysis Error</i> .....	36
Chapter 5: Results of Secondary Studies.....	38
5.1 Effect of Neutralization on Roughness and Morphology .....	38
5.2 Morphology of Wet Chitosan Films .....	39
5.3 Using Raman Spectroscopy to Identify Functional Groups .....	41
5.3.1 <i>Alkane Analysis</i> .....	42
5.3.2 <i>O-H and N-H Analysis</i> .....	44
5.3.3 <i>Amide and Ether Analysis</i> .....	45
5.3.4 <i>Effect of Neutralization on Amine Peak Intensities</i> .....	46
5.4 Determination of Spatial Resolution using Raman Spectroscopy .....	47
Chapter 6: Conclusions.....	52
6.1 Summary of Conclusions.....	52
6.2 Future Work.....	53
REFERENCES .....	55

## LIST OF TABLES

Table 1. Deposition conditions from 2/8/05. ....	16
Table 2. Deposition from 4/13/05.....	17
Table 3. Deposition Conditions from 5/12/05. ....	17
Table 4. Deposition Conditions from 8/17/05.....	18
Table 5. Deposition Conditions from 11/16/05.....	19
Table 6. Films grown with same conditions on the same day yield different thicknesses. .....	23
Table 7. Films thickness does not follow expected results for deposition E. ....	25
Table 8. Roughness increases with current density. ....	30
Table 9. Raman excitation frequencies for functional groups present in chitosan and chitin. The groups listed for chitin are in addition to the groups contained in chitosan with the exception of the primary amine group.....	41

## LIST OF FIGURES

Figure 1. The structure of chitin and chitosan [4].....	2
Figure 2. pH gradient drives deposition of chitosan on WE [10]. .....	7
Figure 3. The combi cell is used for chitosan electrodeposition.....	9
Figure 4. Wafers used for chitosan electrodeposition.....	11
Figure 5. Thickness vs. time for deposition A. ....	21
Figure 6. Thickness vs. current density for deposition B. ....	22
Figure 7. Thickness vs. current density for deposition C. ....	22
Figure 8. Thickness vs. time for deposition D. A: Line of best fit for data with slopes representing growth rate. B: Line of best fit using an intercept of 0 with slopes. C: Line of best fit for growth rate vs. current density shows that the growth rate increases by 2.21 nm/s for every one unit increase in current density. ....	24
Figure 9. Roughness increases logarithmically with scan size. ....	26
Figure 10. AFM images show that roughness increases with thickness for the same current density. All images use the same image processing parameters. ....	28
Figure 11. A (top): Roughness does not show a clear trend when plotted vs. time. B (bottom): Roughness increases with thickness for each current density. ....	29
Figure 12. Roughness and standard deviation vs. thickness for deposition B. A: The roughness vs. thickness curve has an “s” shape. B: Standard deviation increases with thickness indicating increasing heterogeneity. ....	31
Figure 13. A (left): Roughness increased logarithmically with thickness for deposition C. B (right): Normalized roughness decreases with thickness. ....	32
Figure 14. AFM images from chip one of deposition C show that roughness increases with thickness and current density. ....	32
Figure 15. AFM show the nanostructure for films of similar thickness and different current density from deposition E. ....	33
Figure 16. Global thickness vs. time and current density data have large variation.....	35
Figure 17. Dry and wet chitosan films have different morphologies. ....	39
Figure 18. Fluorescent intensity maps demonstrate that dry films are much rougher than wet ones. ....	40
Figure 19. The high wavenumber end of the chitosan spectrum contains alkane, amine, and hydroxyl peaks. ....	43
Figure 20. Methyl peaks present in the chitosan spectrum indicate chitin. ....	44
Figure 21. Amide (green) and ether (purple) peaks in the chitosan spectrum. ....	46
Figure 22. The intensity of amine peaks increases after neutralization. ....	47
Figure 23. Full Raman spectra of chitosan. A: Typical spectrum with peak values. B: Peak intensity increases with film thickness. ....	49
Figure 24. Spatially selective Raman spectra show residues on substrate are not chitosan. .....	50

## LIST OF ABBREVIATIONS AND ACRONYMS

AFM	Atomic Force Microscope/Microscopy
CCD	Charge Coupled Device
CE	Counter Electrode
DD	Degree of Deacetylation
DNA	Deoxyribonucleic acid
H-NMR	Hydrogen (proton) Nuclear Magnetic Resonance (spectroscopy)
IR	Infrared
ITC-irst	Il Centro per la ricerca scientifica e tecnologica
LAMP	Laboratory for Advanced Materials Processing
LPS	The Laboratory for Physical Sciences
MSAL	MEMS Sensors and Actuators Lab
MEMS	Micro-Electro-Mechanical Systems
NHS	N-Hydroxysuccinimide
RMS	Root Mean Square
SEM	Scanning Electron Microscopy
SURF	Laboratory for Surface and Interface Studies
TEM	Transmission Electron Microscopy
WE	Working Electrode
XPS	X-ray Photoelectron Spectroscopy

## Chapter 1: Introduction

Chitosan, an amine-rich polysaccharide composed of N-acetyl-D-glucosamine and D-glucosamine, is being explored as a biocompatible substrate for biological reactions in microfluidic channels. Chitosan is selectively electrodeposited on gold electrodes within the microchannels, forming an interface between inorganic material and biological species used in the device like enzymes, proteins, and DNA. The effectiveness and biocompatibility of the films are affected by the chemical and physical properties of the films; these properties need to be tailored for particular biological applications. For example, large amine site density is favorable for the attachment of biomolecules [1]. However, this condition is toxic to cells [2]. Different cells and molecules also thrive in different surface roughness conditions. These properties are affected by the many parameters in the electrodeposition process.

The growth of electrodeposited chitosan biopolymer is still not clearly understood. Currently, reproducibility of the films is difficult in this complex system that is sensitive to many variables. It is unknown exactly how the deposition parameters affect the physical and chemical properties of the films. The current experimental set up and procedures for chitosan deposition are not optimized and understanding of the growth of chitosan is lacking. This study will primarily examine the effect of current density and deposition time on the surface roughness of chitosan films using Atomic Force Microscopy (AFM). In addition, the chemical functionality of chitosan will be identified using Raman spectroscopy.

## 1.1 Chitosan

The polysaccharide chitosan is being explored as a substrate for biological reactions. Besides advantageous chemistry, chitosan is environmentally friendly, commercially available, and inexpensive. Chitosan is synthesized by the deacetylation of chitin, (1,4)-2-acetoamide-2-deoxy- $\beta$ -D-glucan, the second most abundant natural polysaccharide that is found in insect and crustacean exoskeletons and the cell walls of fungi [3]. The structures of chitin and chitosan are illustrated in Figure 1. At moderately acidic pH (pH < 6), the amine groups of the chitosan become protonated and form positively charged ammonium groups. The conversion from neutral polymer to positive electrolyte means that chitosan will dissolve in a slightly acidic, aqueous solution. However, if a base is added and the pH rises above 6.5, the ammonium groups are deprotonated and converted back to neutral amines, making chitosan insoluble. This property provides for an easy mode of deposition based on the pH dependent solubility of chitosan.

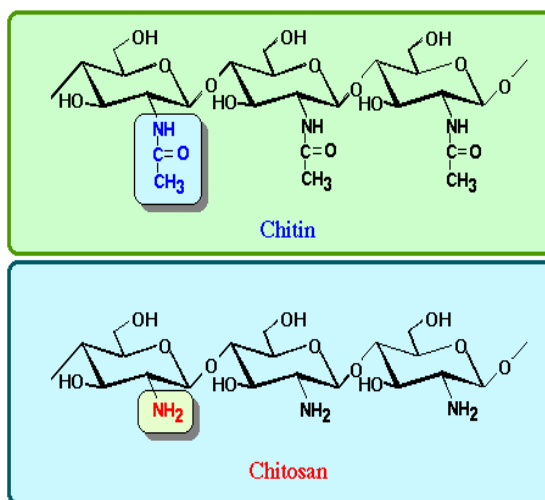


Figure 1. The structure of chitin and chitosan [4].

Chitosan is the common name for chitin which is more than 50% deacetylated. This means that chitosan is really a mix of chitin and chitosan groups within one molecule, but that most of the identifying groups are amine rather than acetyl groups. The structure of chitosan, block or random copolymer, has been debated with no clear answer. However, the structure of the ideal polymers has been agreed upon. Ideal chitin with 0% deacetylation will be flexible and follow a random coil conformation. On the other hand, ideal chitosan that is 100% deacetylated will be a rigid structure due to electrostatic repulsion. The block copolymer structure is composed of sequences of mainly chitin or chitosan sections that alternate throughout the chain. In [5], the block copolymer structure was proposed after viewing TEM images. The authors proposed a ball and chain model consisting of spheres made of flexible coils of mainly chitin separated by rigid chains of mainly chitosan. Ottoy et. al. used H-NMR to study the structure of chitosan [6]. They made calculations of the probability of finding two acetylated or deacetylated monomers in sequence as a function of deacetylation time and compared them with experimental data from H-NMR. They found the experimental data to be very close to their calculations for the random model and to not agree with the block copolymer model. Interestingly, Aida et. al. found both models to be correct by studying chitosan with different degrees of deacetylation (DD). They discovered that the DD affects the type of copolymer formed [7]. In addition, Kurita et. al. found that the method by which the chitosan is prepared affects the structure [8].

## 1.2 Previous Work

In our group, chitosan has been successfully deposited onto gold electrodes with spatial and temporal selectivity. Spatial resolution has been proven down to 20 microns

using fluorescently tagged chitosan and fluorescence microscopy. In addition, chitosan can be fluorescently tagged after deposition by reacting with NHS-fluorescein (5- (and 6)-carboxyfluorescein succinimidyl ester) [9]. Chitosan films have been deposited inside microchannels and have been proven as adequate substrates for biological reactions within them. However, we have not previously studied the materials science of these films and still do not understand how they grow.

Collaborators at ITC-irst in Italy have researched many properties of chitosan. The degree of deacetylation, DD, labels what percentage of the molecule is chitosan versus chitin. Reflecting the composition, this value strongly affects the chemical, physical, and biological properties of the molecule. However, it is difficult to obtain an accurate DD value for a chitosan sample. At ITC-irst, they found that the DD is highly dependent on the analytical mode used so that results from various methods did not often agree with the value provided by the supplier. However, they did find that 100% DD films were very rough and had problems with cell adhesion. This is probably because large amounts of amine groups are toxic to cells, but useful for attaching biological molecules. Thus the DD must be tailored for the appropriate application. In addition, they studied the effect of the deposition method, air dried vs. electrodeposited, and performed studies using actual cells. They found that different cells preferred different film characteristics, but that the cells thrived more on the air dried films. However, using XPS, they found that the surface chemistry was the same regardless of the deposition method. Thus the key to cell adhesion and health must lie in the physical morphology of the films rather than the chemistry and thus the roughness and morphology are the main subject of this research.

### 1.3 Motivation

A microfluidic device with chitosan covered reaction sites is being developed with long-term goals of biosensing, nanostructure assembly, enzymatic reactions, and study of individual cells. This biological MEMS device could be used for quorum sensing, disease diagnosis, and contamination detection. In addition, this technology could be used to assemble tiny structures like carbon nanotubes in a specific manner for molecular electronics [1]. To make these goals attainable, an interface layer between the inorganic substrate and the biological molecules must be implemented. Primary amine groups are critical for attracting biomolecules like proteins and DNA to a surface, making chitosan a likely choice. Overall, the chitosan films need to attract a high density of biomolecules to their surfaces.

## Chapter 2: Experimental

### 2.1 Chitosan Deposition

Growth of chitosan via electrodeposition allows for spatially and temporally selective deposition through the control of voltage or current. Electrodeposition exploits the pH dependent solubility of chitosan; deposition from solution occurs in areas of high pH. A mechanism for chitosan electrodeposition has been proposed by Fernandes et. al. [10]. When a voltage is applied between two electrodes, the positive electrode (hereon called counter electrode or CE) becomes positively charged and the negative electrode (hereon called the working electrode or WE) becomes negatively charged. A local region of high pH is generated electrochemically at the WE surface due to the hydrogen evolution reaction. The reaction rate is proportional to the current density which can be adjusted by changing the applied voltage.

As indicated in Figure 2, the proton consumption at the WE is partially compensated for by protons generated by the dissociation of water. Thus a pH gradient can be initiated in the immediate vicinity of the WE surface depending on the relative rates of hydroxyl ion generation and hydroxyl ion diffusion from the interfacial region [10]. A chitosan molecule that enters the high pH region ( $\text{pH} > 6.3$ ) will become deprotonated and subsequently insoluble, depositing on the WE. No chitosan will deposit on the CE because the pH is above 6.3. However, the gold of the CE dissolves with repeated use likely due to the low pH surrounding the CE and due to electrochemical reactions (Au ions are attracted to the WE so the Au dissolves). While it may be fairly simple to obtain growth, controlling and predicting the growth is very difficult as the growth is sensitive to a large number of experimental parameters.

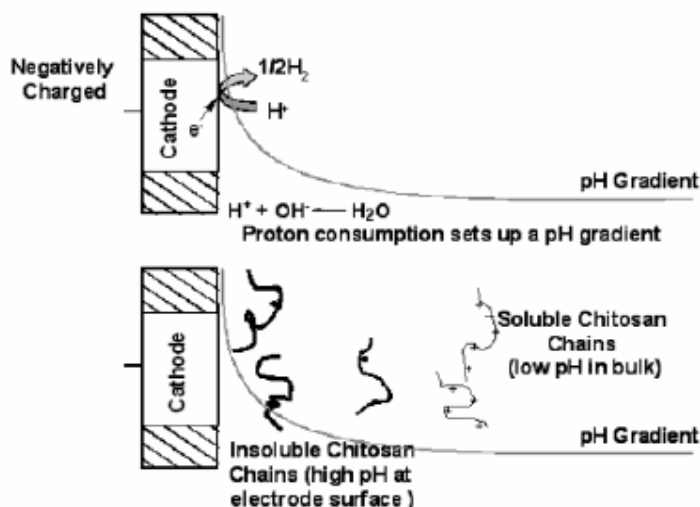


Figure 2. pH gradient drives deposition of chitosan on WE [10].

### 2.1.1 Making Chitosan Solution

To perform electrodeposition of chitosan, the as-received chitosan flakes must be synthesized into a polyelectrolyte solution. The solution of chitosan must be prepared very carefully since characteristics like pH, molecular weight, and concentration (salt and chitosan) significantly affect the properties of the final film. Derived from crab shells, the chitosan was obtained from Sigma-Aldrich as minimum 85% deacetylated flakes with an average molecular weight of 370,000. The flakes are then ground up to increase the surface area and to allow for faster dissolution. Next the graduated cylinder and pH meter are calibrated and 2M HCl is formulated. Both precisely measured, the ground chitosan is added to deionized water while stirring magnetically with a stir bar. Monitored by a pH meter, 2M HCl is dripped from a burette into the mixture slowly to decrease the pH to between 2 and 3 since chitosan dissolves fastest in that range. The addition of HCl is interrupted once the pH reaches the desired level and the amount of acid added is recorded for the purpose of calculating the ion concentration. The solution is then stirred

until the chitosan is nearly dissolved, usually after about 8 hours. Next the solution must be filtered to remove the insoluble impurities that were present in the flakes. After vacuum filtration, 1M NaOH is added to the solution in order to raise the pH to a suitable range for deposition (~5). It is important to add NaOH slowly and in small drops since very high local pH causes chitosan precipitates that could lead to the need for more filtering. Lastly the concentration is calculated. The solution must be kept cold in a refrigerator to avoid the growth of fungi. However, the solution must warm to room temperature before performing the deposition.

The chitosan solution used for deposition is critical since factors like ion concentration and pH affect the final properties of the film. Ion concentration is important because it affects the conformation of the chitosan molecules (affects the energy favorability) and the electrical properties (ions are conductive). The acidic chitosan solution is conductive because the chitosan molecules become protonated at low pH, making them positively charged. During deposition, a current is set up between the counter and working electrodes. Moreover, additional ions, like  $H^+$ ,  $Na^+$ , and  $Cl^-$  are present due to the chitosan solution preparation. As with the protonated chitosan, they are charged and they are conductive. The more charge carriers or the greater the density of the carriers, the less resistance that is present so that less voltage is needed to produce a steady current, affecting the effective current for a given voltage and thus the electrical data. Therefore the concentrations and amounts of acids and bases added while making the solution must be carefully monitored. In addition, ion concentration can affect the conformation of the molecules since polymers are very sensitive to their environments. In a good solution, it is favorable for the polymer to spread out in the solution, making it

long and fiber like. However, in a bad solution, contact with the molecule itself is preferred over the solution. This means that the molecules will ball up into spheres to minimize contact with the energetically unfavorable solution. Thus the interaction between the polymer (chitosan) molecules and the solution (water, HCl, NaOH) affects the conformation and thus morphology of the film.

### 2.1.2 Chitosan Deposition

Deposition was performed in SURF for all of the depositions except for the last which was done in LAMP. Deposition is performed in a chamber call the “combi cell” (for combinatorial cell as it was designed to test a matrix of experimental parameters) as pictured in Figure 3. This in-house designed and built apparatus is set up for *in situ* electrical and optical measurements during deposition. Two computers running LabView are used to monitor and record this data. The LabView programs were created by Jung Jin Park.

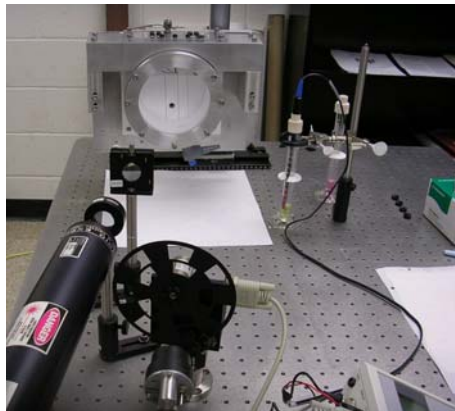


**Figure 3. The combi cell is used for chitosan electrodeposition.**

For deposition, a wafer is loaded into the clip containing push pin electrical contacts. The contacts connect the electrodes to the negative side of the power supply.

The Pt wires, the counter electrodes, are attached to the positive side. A reference electrode is also used. The chamber is then filled with chitosan to cover the electrodes. During deposition the laser beam hits the electrode to monitor changes in the reflectivity. A pH meter reads the pH and temperature, while LabView records the electrical data. The electrical measurements tell the operator whether the film is depositing correctly. A good signal is signified by a large, steep increase in the voltage needed to maintain the constant current in the first few seconds followed by a very slight, steady increase in the voltage. This is because in the first stage, the electrical path is being initiated and then the resistance is increased gradually by the growth of the partially insulating film.

Deposition occurs on substrates made from silicon wafers and subsequent microprocessing techniques. Three chips are made from a single 4" silicon wafer with a 500 nm oxide layer. Patterns are created by photolithography. The electrodes consist of a 5 nm Cr adhesion layer and 200 nm of Au. Au is used because it is inert, stable, and easily processed. The working electrodes are squares that are 1 cm x 1 cm as illustrated in Figure 4. Microwires connect the electrodes to the contact pads. Contact is made using push pins which are connected to mini banana plug sockets. The banana plugs then go to the back of the combi cell where the wires are connected to alligator clips from the power supply. Built into the combi cell are also ports for the reference electrode and for the pH meter. The counter electrodes consist of three Pt wires.

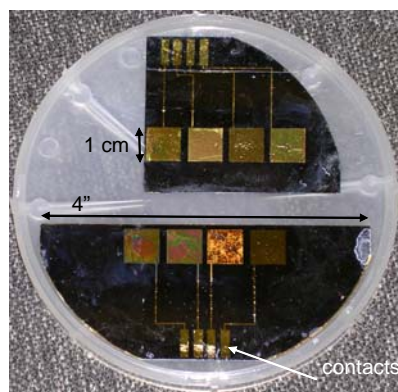


**Figure 4. Wafers used for chitosan electrodeposition.**

## 2.2 Film Characterization

### *2.2.1 Film Thickness*

Dry thicknesses were measured by Jung Jin Park and Susan Beatty in MSAL using a Dektak mechanical stylus profiler by Veeco. The profiler traces the surface in a single line scan of user-defined length. Since the thickness often varies across the film from top to middle to bottom, multiple scans are useful to determine an average thickness. Unfortunately, the scans were not always done the same number of times for each electrode. Some were scanned only once while others were scanned four or more times. The actual film thickness was recorded as the average difference in the heights (from top of the film to bare SiO<sub>2</sub>) minus the thickness of the electrode, 205 nm.

### *2.2.2 Atomic Force Microscopy*

Two different AFMs were used for quantitative roughness measurements and imaging the surface morphology. Both were used in tapping mode with silicon tips with a resonance frequency around 250 kHz. The first AFM that was used is located at the Laboratory for Physical Sciences in the Surface Characterization lab, room 1221A. It is a

Dimension 3100 made by Digital Instruments of Veeco Metrology. The other AFM that was used is a Dimension 5000 located in Professor Michael Fuhrer's lab in the physics building, room 2219. Both of these instruments can accommodate samples up to 8" in diameter and 12 mm thick in air, vacuum, or fluids. A He-Ne laser beam is reflected off the cantilever and detected by a quadrature optical detector to determine the precise oscillation of the cantilever. The scanner head is a piezoelectric tube scanner capable of up to 90 x 90 micron scans with 1% lateral accuracy and a 6.7 micron vertical range. In addition, the AFM includes an optical microscope with 1.5 micron resolution for ease of navigating the surface [11]. Further specifications for these instruments can be found online on the Veeco Products website at <http://www.veeco.com>.

AFM scans were performed in air on dry films. Naturally, wet analysis would be preferred since the films are used in wet conditions and polymers are highly sensitive to their environment. However, tapping AFM in fluid is extremely challenging and requires special adapters and a different, more expensive kind of tip. In addition, resolution is decreased in water versus air. Therefore, tapping in air is the best method for performing roughness measurements. Scans were performed in sizes ranging from 500 nm to 50  $\mu\text{m}$ . After some experience, 2  $\mu\text{m}$  scans were deemed the best for optimization of scale, resolution, and time. All roughness calculations were made using the Nanoscope software provided with the microscopes. The equations used to calculate the roughness values are:

- The RMS ( $R_q$ ) roughness is the standard deviation of the z values,

$$R_q = \sqrt{\frac{\sum_{i=1}^N (Z_i - Z_{av})^2}{N}}$$

- The mean roughness ( $R_a$ ) is the arithmetic average of the deviations from the center plane,

$$R_a = \frac{\sum_{i=1}^N |Z_i - Z_{cp}|}{N}$$

- $R_{max}$  is the difference in height from the highest to the lowest points on the surface relative to the mean plane. It is not as useful as the other calculations because the films are so heterogeneous that it is not a good measure of roughness.

In accordance with industry standards, the images are flattened before calculations are made. For all samples, a third order flatten was applied to the image. More information about this operation can be found in the D5000 software manual, p. 105.

The resolution acquired by the AFM is dependent on many factors, some of which can also affect the roughness data. First is the size or radius of curvature of the tip. The smallest lateral feature size that can be imaged is limited by the tip size. The tip size often increases with use as it picks up dirt and dust from the atmosphere and from the sample. In addition, the sidewall angles of the tip and sample features affect the resolution of sharp features. The user can partially control the vertical ( $z$ ) resolution by lowering the  $z$  limit. Since points can only be taken in discrete intervals, lowering the  $z$  limit lowers the interval size, gaining in resolution. However, the  $z$  limit must exceed the maximum feature size to avoid crashing the tip into the sample. Similarly, lateral resolution is affected by scan size and the number of points taken in one direction (128, 256, 512). For example, for a 50 x 50  $\mu\text{m}$  scan that has 512 pixels, 98 nm is the maximum feature size

resolved. Moreover, noise especially from external vibrations can also limit the resolution in all three dimensions.

### *2.2.3 Raman Spectroscopy*

The Raman microscope is located at LPS in room 1208, the Organic Electronics lab. The HoloSpec Raman microscope used was made by Kaiser Optical Systems. It consists of HoloLab 5000 modular Raman spectrometer, a Leica microscope, and CCD camera. The spectrometer is a holographic notch type system, meaning that it acquires data quickly and all at once rather than by scanning the surface line by line. Because of this, it is faster but with a lower resolution than other types of systems. This microscope has a resolution of 4 k (wavenumbers). Exposure time and number of accumulations were increased until a spectrum was attained with good resolution, a high number of counts, and low noise. Exposure time was 40 seconds for each of four accumulations. Analysis of the peaks was performed using the HoloGRAMS software by ThermoGalactic. The He-Ne laser sampling area is 1  $\mu\text{m}$  in diameter and 2  $\mu\text{m}$  in depth. This means that the intensity of films thinner than this will be proportional to thickness due to the number of scattering centers scaling with thickness.

## 2.3 Hypotheses

Based on what I knew about the deposition process and from reading previous results, I made several hypotheses and subsequently chose deposition parameters to help explore them. First, films with higher current density should be rougher than those grown with a lower current density. This is because with a high current density, many molecules are approaching the surface quickly. They should be less efficiently arranged because

they do not have time to arrange in an ordered fashion or to “fill in the holes.” Upon drying, they have more room for collapse, creating large trenches and ridges. In addition, hydrogen evolution is greater due to increased reaction rates, producing more bubbles in the film. The hydrogen does not have as long to diffuse because the film grows faster and thicker and so it gets trapped in the chitosan films, making them rougher and full of bubbles. Thus this film should have a lower density than one grown at a lower current density. The small current density films should be smoother, denser, and more efficiently packed because the deposition occurs at a slower rate and the film has time to relax.

The roughness and morphology should be different for wet and dry films. When the film is wet, the molecules are swollen full of water. As the film dries, the water evaporates and the structure collapses in a rather random manner. The collapse makes the dry film rougher and more heterogeneous than when it was wet. Also, in wet conditions, the hydrogel-like films interact with the water, meaning that water is a favorable solution for chitosan. This means that the film should be rather fibrous since the chitosan will be in a good solution, spreading out with a large pervaded volume, especially because of residual  $\text{NH}_3^+$  groups that provide for electrostatic repulsion. As the film dries, the molecules collapse and should want to minimize their surface area, forming spheroids.

#### 2.4 Experimental Parameters

Several chitosan depositions were performed using different experimental parameters to determine their effect on the roughness. The conditions are described below for each. For simplicity, each deposition will be referred to by letter rather than date of deposition (present in each sub-heading) in the remaining chapters.

#### 2.4.1 Deposition A: 02/08/05

The goals of this deposition were to study the effect of time, current density, and neutralization. Films were studied using AFM and Raman both before and after neutralization with 1M NaOH. The parameters are shown in Table 1 below. This experiment was a great learning experience for developing the characterization parameters.

**Table 1. Deposition conditions from 2/8/05.**

<b>Electrode #</b>	<b>Current Density (A/m<sup>2</sup>)</b>	<b>Time (s)</b>
1	5	240
2	5	180
3	5	120
4	5	60
5	4	240
6	4	180
7	4	120
8	4	60

#### 2.4.2 Deposition B: 04/13/05

The goal of this deposition was to examine how current density affects films grown for the same amount of time as shown in Table 2. In addition, some finer points were studied like the homogeneity across an electrode, the effect of current density on homogeneity, the average roughness measured from day to day, and the effect of scan size on roughness.

**Table 2. Deposition from 4/13/05**

<b>Electrode #</b>	<b>A/m<sup>2</sup></b>	<b>Time (s)</b>
8	8	180
7	7	180
6	6	180
5	5	180
4	4	180

*2.4.3 Deposition C: 05/12/05*

This deposition is a continuation of deposition B to get more data for the smaller current densities because during deposition B, something went wrong for the 1-3 A/m<sup>2</sup> electrodes and no deposition was recorded. This low current density region is most useful in practice for depositing in microchannels. This deposition conditions for C are found in Table 3 below

**Table 3. Deposition Conditions from 5/12/05.**

<b>Electrode #</b>	<b>A/m<sup>2</sup></b>	<b>Time (s)</b>
1	1	180
2	2	180
3	3	180
4	4	180
5	1	180
6	2	180
7	4	180
8	6	180

*2.4.4 Deposition D: 08/17/05*

Deposition D was used solely to gain more information about thicknesses as a function of current density and time. More data from the lower current densities was

needed to plan parameters for the next deposition to have constant thickness in order to ultimately determine the effect of current density on roughness independent of thickness.

The conditions are shown in Table 4.

**Table 4. Deposition Conditions from 8/17/05**

<b>Electrode #</b>	<b>A/m<sup>2</sup></b>	<b>Time (s)</b>
1	3	240
2	3	180
3	3	120
4	3	60
5	2	480
6	2	420
7	2	360
8	2	300
9	2	240
10	2	180
11	2	120
12	2	60
13	5	120
14	5	60
15	4	120
16	4	60

#### *2.4.5 Deposition E: 11/16/05*

The goal of deposition E was to create films of the same thicknesses but with different current densities. Data taken from deposition D was used to try to create films with the same thickness on each wafer. The goal for wafer 1 was 800 nm and for wafer 2 was 1  $\mu\text{m}$ . The conditions used are presented in Table 5. A broken lead prevented

deposition on electrode 7 and no deposition was recorded on electrode 1 due to power supply problems.

**Table 5. Deposition Conditions from 11/16/05**

<b>Electrode #</b>	<b>A/m<sup>2</sup></b>	<b>Time (s)</b>
2	2	160
3	3	120
4	4	90
5	2	200
6	3	155
8	4	120

*2.4.6 Deposition F: 02/09/06*

Deposition A conditions were repeated exactly (see Table 1) but this time with the goal of wet characterization in the AFM. The goal was to compare wet and dry roughness and morphology for a variety of thicknesses using the middle current densities to study the growth of chitosan.

## Chapter 3: Thickness vs. Time and Current Density

Affected by experimental conditions, the thickness is an important result that also affects other properties of the film. It was reported by Wu et. al. that the growth of chitosan films is non-linear with time [12]. We found that it is approximately linear over small, intermediate times. If the thickness is plotted versus the deposition time, the current density influences the slope of the line; the slope should increase with increasing current density. However, from deposition to deposition, this slope was not the same for the same current density; the results were not repeatable from day to day. Also, the measured dry thicknesses did not always follow even the very basic, expected trends; there were points that did not make scientific sense at all. However, data generally follows as predicted: for the same time, films grown with a higher current density will be thicker than those grown at a lower current density and increasing the time of deposition will increase the thickness of the film.

### 3.1 Deposition A

In deposition A, 6 of the 8 electrodes were shown to have deposition. Electrode 4 had no deposition due dissolution from being left in the chamber as confirmed by profilometry and AFM. Electrode 6 showed no deposition from the profiler results, but something was on the surface according to the AFM images though it did not look like chitosan. Thus both of these electrodes are left out of all remaining analyses. The 5 A/m<sup>2</sup> substrate followed an expected linear trend, but the 4 A/m<sup>2</sup> substrate had very unexpected results as shown in Figure 5. The thicknesses measured on the 4 A/m<sup>2</sup> substrate did not make sense because for the same current density, as time increased, the film should increase in thickness because more molecules are being added to the film. There is no

possibility that dissolution, the competing force, is faster at this current density.

However, in the  $4 \text{ A/m}^2$  substrate, the 60s sample was thicker than the 120s sample by almost 50%. In addition, electrode 7 was thicker than electrode 3, even though 7 had the same time with a smaller current density. The current density increases the attraction and flow of molecules to electrode, increasing the thickness, or at least the density of the films. This specimen did not follow past results or logic.

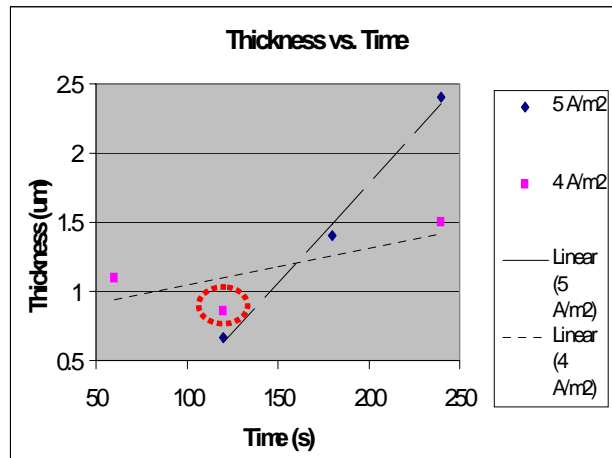
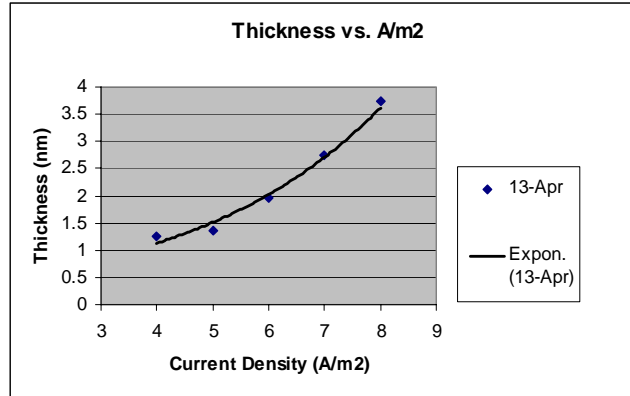


Figure 5. Thickness vs. time for deposition A.

The  $5 \text{ A/m}^2$  substrate grew as expected with a growth rate of  $14.4 \text{ nm/s}$  using the slope of the linear fit. Using an intercept of 0, the slope becomes  $8.7 \text{ nm/s}$ . The slope is  $2.7 \text{ nm/s}$  for the  $4 \text{ A/m}^2$  data, and is  $7 \text{ nm/s}$  with a set intercept at (0,0).

### 3.2 Deposition B

The thicknesses for deposition B were readily fit with an exponential curve for thickness vs. current density. This exponential increase for a constant time is expected. The data is plotted in Figure 6. Due to experimental errors, no deposition was recorded on the first three electrodes with low current densities.



**Figure 6. Thickness vs. current density for deposition B.**

### 3.3 Deposition C

The thicknesses for deposition C did not correlate well with either an exponential or linear regression line for thickness vs. current density. This may be because here lower to medium current densities are included versus the middle to high range represented by deposition B. This plot is seen in Figure 7. One can also observe that the thicknesses are not repeated from chip one to chip two as shown in Table 6. This data shows the unrepeatability of the results and thus how difficult it is to compare data from deposition to deposition because even in the same day, data is so different (75 - 250 nm differences). This data from the same day with the same conditions show how complex and subject to error the deposition is.

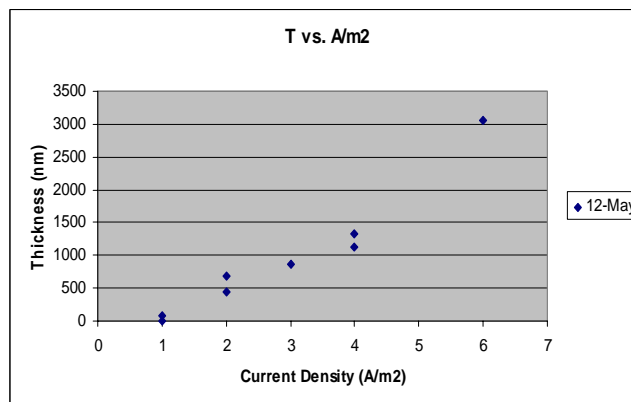


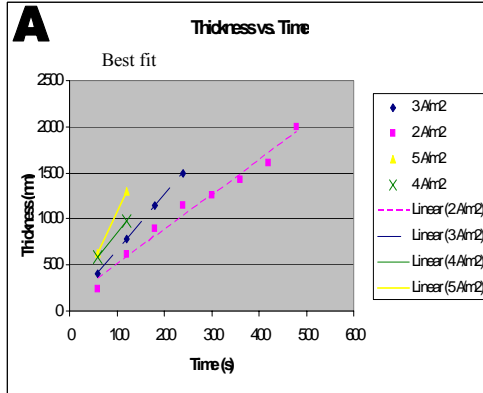
**Figure 7. Thickness vs. current density for deposition C.**

**Table 6. Films grown with same conditions on the same day yield different thicknesses.**

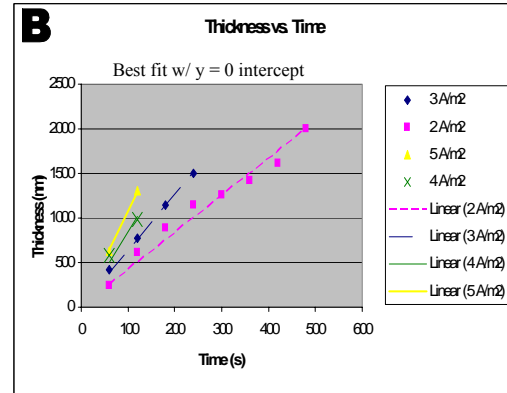
<b>Time</b>	<b>A/m<sup>2</sup></b>	<b>Chip 1 thickness</b>	<b>Chip 2 thickness</b>	<b>Difference (t<sub>2</sub> - t<sub>1</sub>)</b>
180	1	10	85	75
180	2	433	675	242
180	4	1125	1325	200

### 3.4 Deposition D

More films were grown in this deposition than usual to get a large amount of data on the lower current densities and to have it all from the same day due to larger variations in data from different depositions. The data from deposition D show how current density affects the slope of the thickness vs. time graph known as the growth rate. In Figure 8a, the thickness vs. time data is presented with linear fits with the slopes given. However, the slope values make more sense when an intercept of (0,0) is added and used as shown in Figure 8b. The growth rates for each current density are given and show how the intercept addition affects that value advantageously. This is explicit in Figure 8c which plots the slopes calculated in 8a and 8b for each current density. It is obvious that the (0,0) intercept data is more believable. Also the increase in growth rate is linear with current density, increasing by 2.21 nm/s for every one unit increase in current density. With this set of data, it is obvious that the growth rate depends strongly on the current density.



A/m2	Slope (nm/s)
2	3.8
3	6
4	6.6
5	11.2



A/m2	Slope (nm/s)
2	4.15
3	6.33
4	8.46
5	10.8

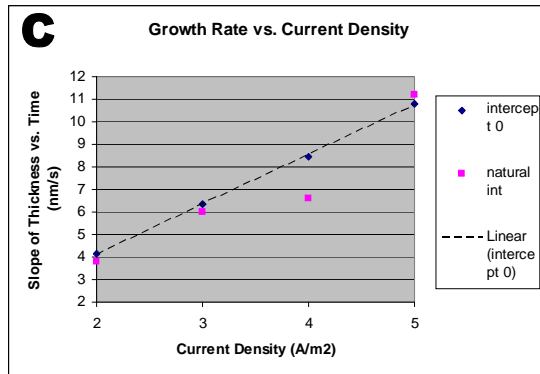


**Figure 8. Thickness vs. time for deposition D. A:** Line of best fit for data with slopes representing growth rate. **B:** Line of best fit using an intercept of 0 with slopes. **C:** Line of best fit for growth rate vs. current density shows that the growth rate increases by 2.21 nm/s for every one unit increase in current density.

### 3.5 Deposition E

This deposition was a total anomaly and has no explanation. To start, the thicknesses were much smaller than the expected 800 and 1000 nm for each chip as shown in Table 7. This experiment again shows that conditions used previously do not necessarily produce the same results when used again. What is worse about this experiment is that for the same time of deposition, the lower current density film was thicker. At least for each current density, the film that grew the longest was the thickest.

Three of the films, shown in red in the table below, will be studied further since they have about the same thickness of 400nm.

**Table 7. Film thickness does not follow expected results for deposition E.**

<b>Electrode #</b>	<b>A/m<sup>2</sup></b>	<b>Time (s)</b>	<b>Film Thickness (nm)</b>
2	2	160	159
3	3	120	418.75
4	4	90	188.3333333
5	2	200	383.75
6	3	155	651
8	4	120	401.25

## Chapter 4: Roughness vs. Thickness

### 4.1 The Effect of Scan Size

After examining the quantitative roughness data from deposition A, it was apparent that scan size was crucial to the interpretation. All of the 50  $\mu\text{m}$  scans had much higher roughness values than all of the 5  $\mu\text{m}$  scans, regardless of the deposition conditions. The hypothesis that roughness increases with scan size was further explored by analyzing a sample from deposition B. AFM scans were executed with scan sizes ranging from 500 nm to 50  $\mu\text{m}$  without moving the lateral position of the sample with respect to the scanner. The roughness was then plotted as a function of scan size as shown in Figure 9. The increase is logarithmic which means that increasing the scan size has a much larger effect on the roughness at small scan sizes whereas an equal incremental increase when using larger scan sizes will have less effect. This effect is likely because increasing the scan area increases the probability of finding a defect like a very low or high spot, dust, or a crater or bubble.

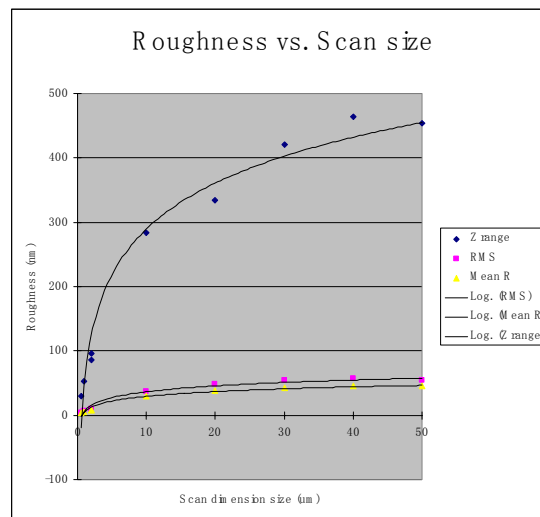


**Figure 9. Roughness increases logarithmically with scan size.**

## 4.2 Deposition A

When observing surface images with increasing time, it was apparent that the roughness increased as shown in Figure 10. The roughness values increased when plotted versus time for the 5 A/m<sup>2</sup> films, but did not show a clear trend for the 4 A/m<sup>2</sup> (Figure 11a) due to the anomaly in the thickness vs. time data. Since thickness also increases with time, the roughness was plotted against the thickness for each. An increasing trend was observed when all roughness values were plotted versus thickness because this normalization resolved the anomaly in the 4 A/m<sup>2</sup> thickness vs. time data. In Figure 11b, roughness vs. thickness was plotted for each current density according to scan size and type of roughness. However, the dependence is not clear with so few data points and such a small range of thicknesses; the dependence could be linear, parabolic, or logarithmic. To determine an accurate correlation, more data is needed that uses the same scan size on multiple locations on each electrode to account for the heterogeneous nature of the surfaces.

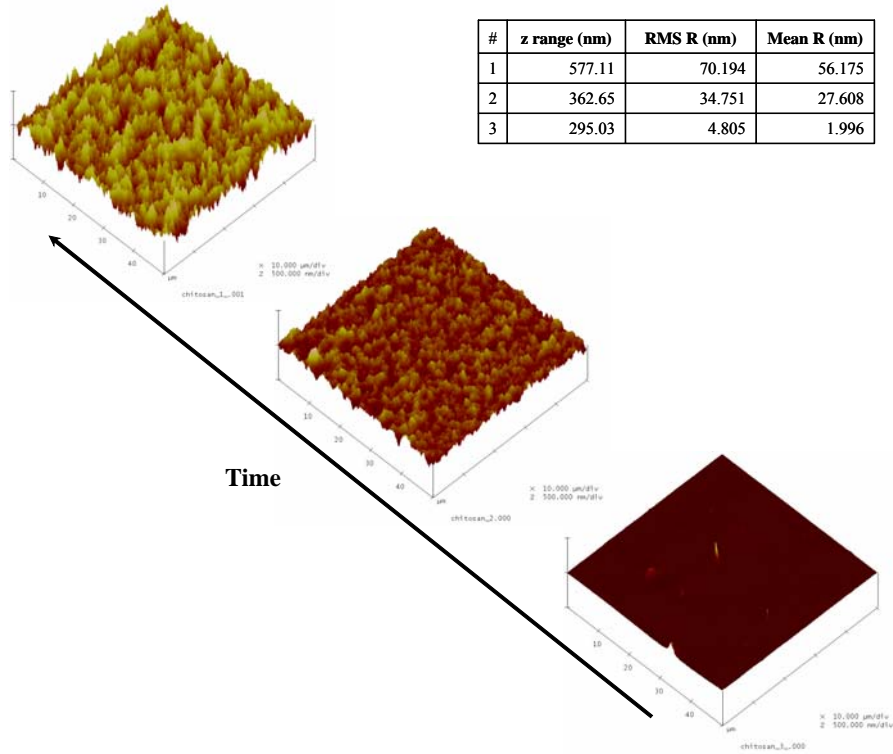


**Figure 10. AFM images show that roughness increases with thickness for the same current density. All images use the same image processing parameters.**

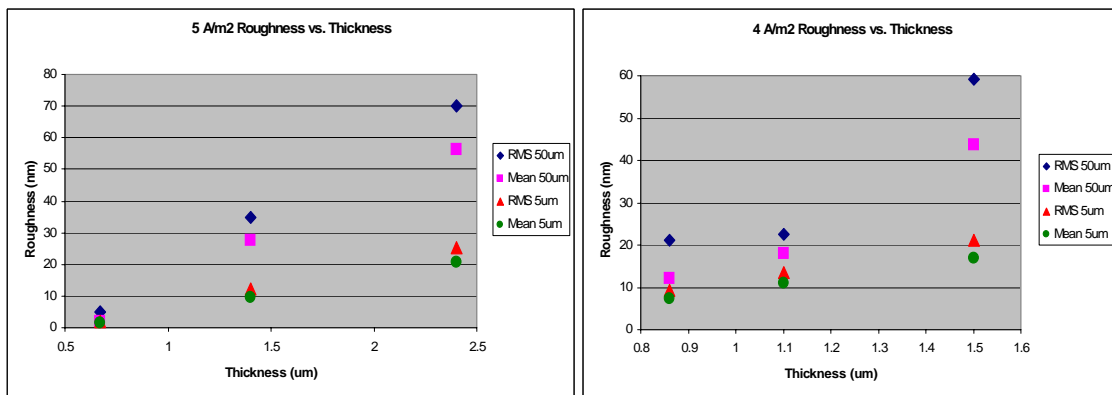
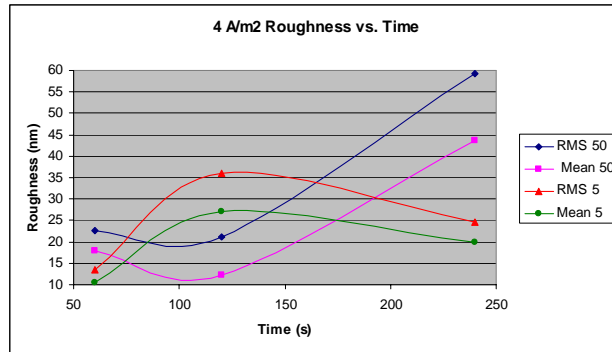


**Figure 11. A (top): Roughness does not show a clear trend when plotted vs. time. B (bottom): Roughness increases with thickness for each current density.**

At this point it was uncertain that increasing current density increases the roughness because increasing the current density increases the thickness. Because roughness seems to depend on thickness and thickness is dependent on deposition time, the effect of current density on roughness cannot be obtained for films grown for the same deposition time. However, in deposition A, two films were close in thickness, electrode 2 on the 5 A/m<sup>2</sup> chip and electrode 5 on the 4 A/m<sup>2</sup> chip with 1.2 μm and 1.3 μm respectively. In this one comparison, the lower current density, despite being slightly thicker, had lower roughness values as presented in Table 9. These data collaborate the theory that films grown with higher current densities are rougher. However, this is one

small area on two different (and heterogeneous) samples. Further research must be conducted to deduce a solid conclusion. To more completely determine the effect of the current density, multiple films must be grown to the same approximate thickness with varying current densities. However, this is hard to predict since the packing efficiency and density will affect how much the structure collapses as it dries and because quantitative results have not been repeatable.

**Table 8. Roughness increases with current density.**

<i>Current Density (A/m<sup>2</sup>)</i>	<b>4</b>	<b>5</b>
<i>RMS (nm)</i>	35	59
<i>Mean R (nm)</i>	27	43

#### 4.3 Deposition B

Using what was learned from deposition A, multiple scans were performed using the same scan size on each electrode. In addition to providing a larger sample size, this allowed for comparison of homogeneity across an electrode by comparing the standard deviations of the values. The average roughness for each thickness is plotted in Figure 12a. Here the trend resembles an “s”, where the roughness increases logarithmically at small to medium thicknesses and then quickly increases for large thickness. For these medium thicknesses represented here, the change in roughness is not very large.

Unfortunately, small thicknesses were not successfully deposited in this deposition and the largest thickness was not easily analyzable. Only one scan was successful on the 8 A/m<sup>2</sup> electrode. It was difficult to engage the tip and once engaged to get a good image because the sample surface was so rough. Thus the one value obtained was thrown out since an average over many scans could not be obtained. In Figure 12b is the standard deviation of the measured values about the average. The standard deviation is a measure

of the homogeneity; a larger standard deviation means that the film is more heterogeneous because the roughness varies more across the electrode. This plot shows that the middle thicknesses have about the same degree of heterogeneity, but that the thick film is highly heterogeneous. This result strongly agrees with optical images of the films as well as the AFM images.

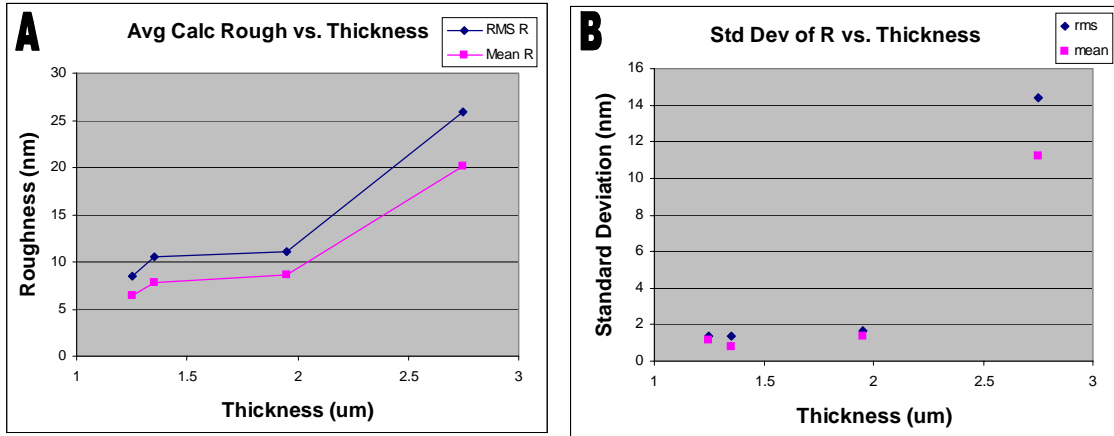


**Figure 12. Roughness and standard deviation vs. thickness for deposition B. A: The roughness vs. thickness curve has an “s” shape. B: Standard deviation increases with thickness indicating increasing heterogeneity.**

#### 4.4 Deposition C

The roughness was plotted against the thickness for deposition C in Figure 13a. The observed trend was logarithmic over all present thicknesses. This trend is in agreement with the previous. It follows that roughness increases quickly with small gains in thickness in the beginning of growth, and that roughness increases much slower for median thicknesses. When roughness was normalized by thickness as in Figure 13b, the normalized roughness decreased with increasing thicknesses. In addition, it was observed from the AFM images that average roughness increased with thickness and current density as shown in Figure 14.

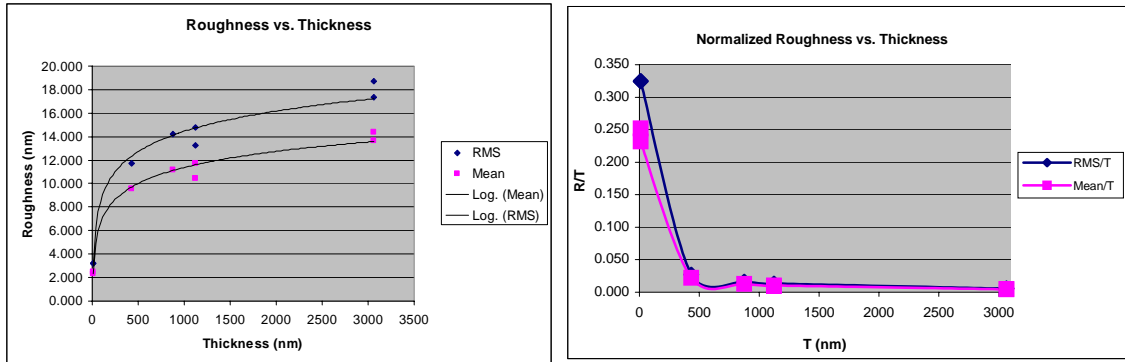


**Figure 13. A (left): Roughness increased logarithmically with thickness for deposition C. B (right): Normalized roughness decreases with thickness.**

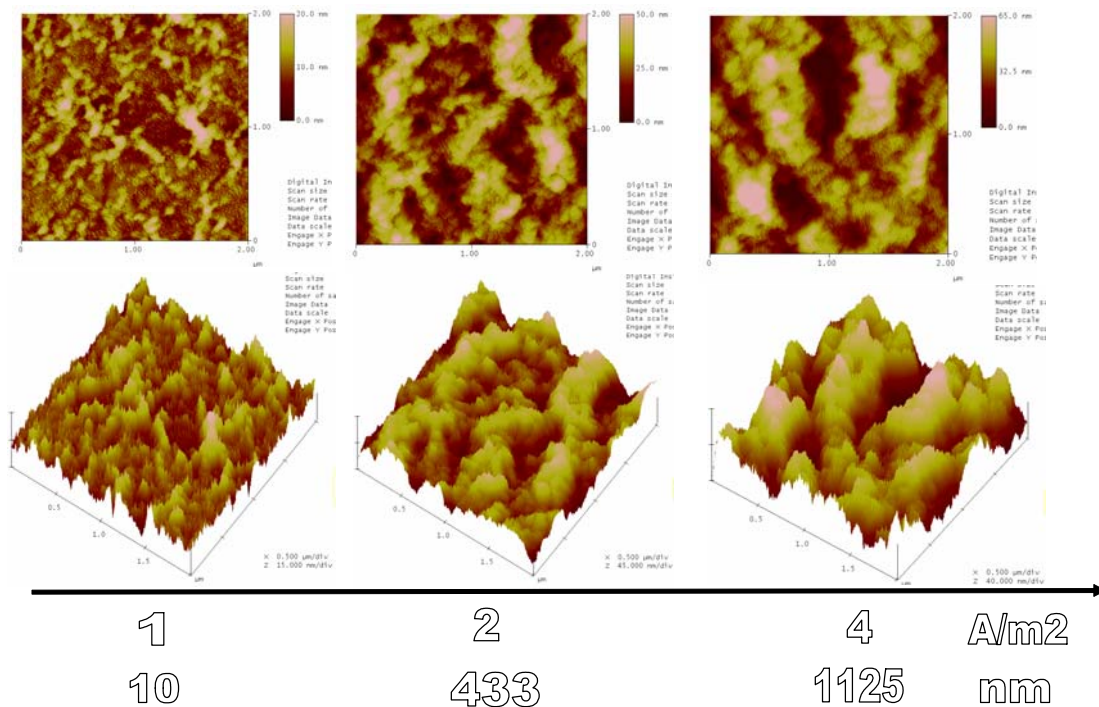


**Figure 14. AFM images from chip one of deposition C show that roughness increases with thickness and current density.**

#### 4.5 Deposition E

Even though deposition E was an anomaly and did not turn out as planned from deposition D, the experiment can be salvaged because of the six films, three had approximately equal dry thicknesses. Two of these three films had a similar roughness,

but the other was much rougher as pictured in Figure 15. Electrode 3 was rougher than 8 which was rougher than 5 which goes in order of thickness, even with only nominal differences in thickness. However, there was no logical trend for the effect of the current density. It follows that the 2 A/m<sup>2</sup> sample (5) would be the smoothest, but the 3 A/m<sup>2</sup> (3) throws it off since it was much rougher than the 4 A/m<sup>2</sup> (8) sample that should have been the roughest. It is especially strange that 3 was rougher than 8 since it was grown with the same deposition time yet lower current density.

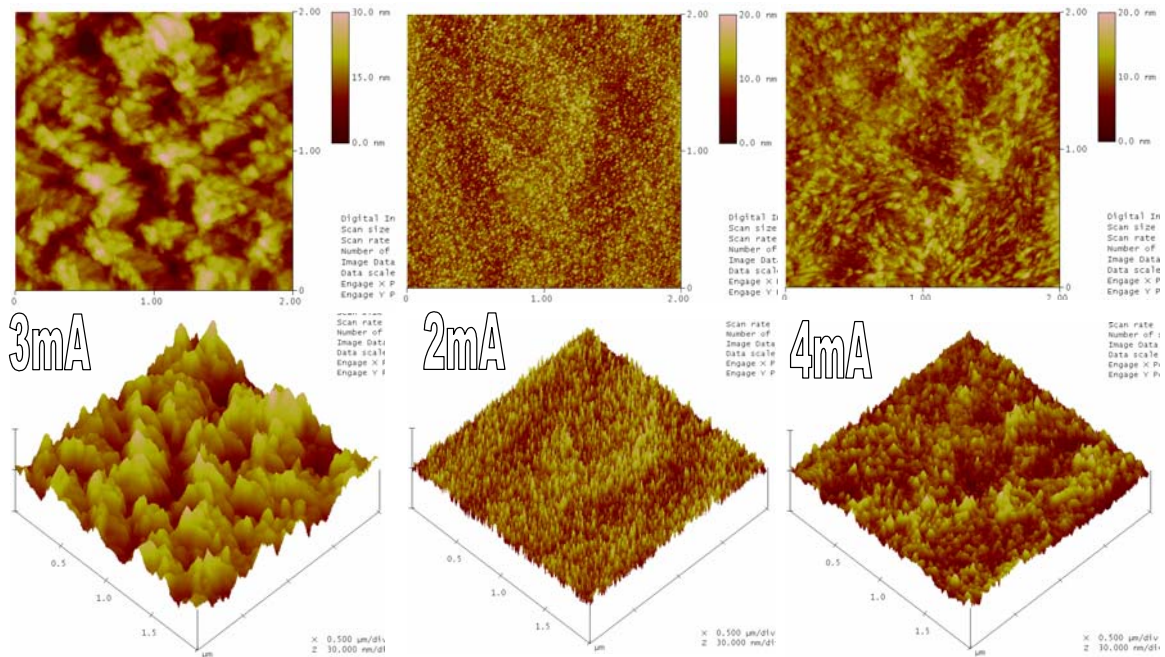


**Figure 15. AFM show the nanostructure for films of similar thickness and different current density from deposition E.**

Since the data for all six films was illogical it is likely that experimental errors contributed to the ill-fitting data that often followed the opposite of all previous results. For example, films that were supposed to have the same thickness varied widely, roughness actually decreased with thickness, and thicknesses were all much lower than

predicted. We have had problems with the power supply and it is possible that it malfunctioned throughout this deposition.

#### 4.6 Discussion

Chitosan is an extremely complex and difficult molecule to work with. It is hard to predict and reproduce its behavior. The growth of amorphous chitosan films is nonlinear for both the thickness and the roughness. Examining the data from individual experiments, it appears that roughness increases logarithmically for small to medium thicknesses. For medium thicknesses, the increase is small and constant in slope and sometimes almost flat. For thick, hydrogel-like films, the increase in roughness is quick and abrupt, appearing exponential. Qualitatively, thick films are very rough and heterogeneous. However, there is not enough quantitative roughness data on hydrogel films to make a solid conclusion. When fitting together the shapes and trends from all the depositions together, the result is an “s” type curve for roughness vs. a large range of thicknesses.

The data support a nucleation or “run away” growth model. Presumably, the first chitosan molecules are attracted to electrical charge concentrations caused by “bumps” on the gold electrode and then subsequent molecules are further attracted to the now larger “bumps.” This nucleation type growth causes the roughness to increase very quickly in the beginning of the growth. Eventually the mounds of chitosan grow into each other and the growth of the film’s roughness begins to slow and level off, making the normalized roughness decrease with thickness.

One major disappointment was the inconsistency of results from deposition to deposition. It would have been nice to have grown more films in one deposition, but

growth is very time consuming; the combi cell cannot be left unattended. Growing just 8 films takes all day even if everything goes nearly perfectly. When the data from all the depositions were plotted together to increase the sample size, the trends were less clear as the plots were very scattered. It was obvious that roughness increased with thickness, but how was not clear. Thickness increased with current density and time as expected, but there were tremendous variations as shown in Figure 16. When plotting roughness vs. thickness, the scatter is similar and in some cases worse because the error is propagated and also added to from the addition of the roughness measurements.

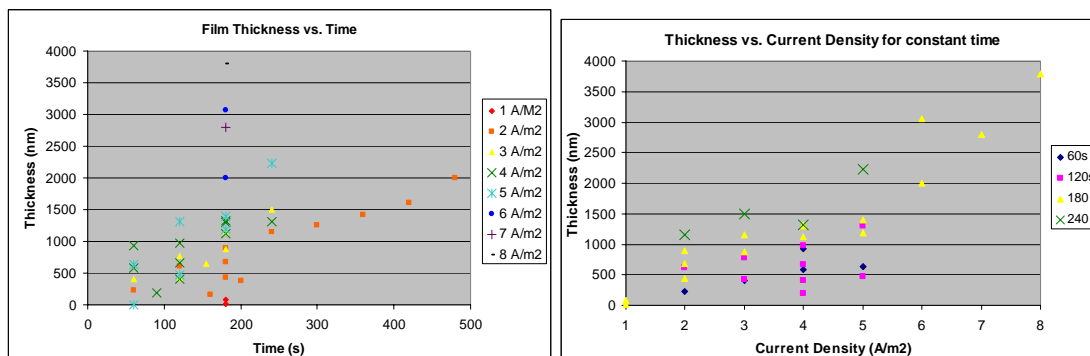


**Figure 16. Global thickness vs. time and current density data have large variation.**

#### 4.6.1 Deposition Error

There are many possibilities for why the data vary so drastically. First off, chitosan itself is very complex and unpredictable. It is polydisperse, varying largely in molecular weight, and has an undetermined structure (block or random copolymer?). Chitosan film growth is sensitive to pH, temperature, concentration, molecular weight, ion concentration, and especially sensitive to small electrical changes. Freshly deposited chitosan dissolves back into the solution ( $\text{pH } 5 < 6.3$ ). Thus the total time the film is in the solution affects the thickness to some degree (the dissolution rate was not studied).

Not only do the films sit in solution while others deposit (deposition is not parallel), but there is also usually at least 5 to 10 minutes between depositions as the laser position is moved, the reflectivity setup is prepared, and the data is saved. In the first few depositions where Jin and Susan chose the parameters, the shortest deposition was done first for constant current density, and for constant time, the smallest current density was first. For later depositions, I chose the order and had the theoretically thickest films deposited first down to the thinnest to equalize the percent dissolved as best as possible. This dissolution and order effect could have significantly affected the results.

Because chitosan solution is so time consuming to make, for each deposition the chitosan is reused. The chitosan is poured into the reaction chamber and after deposition it is put back into the original container. Chitosan molecules are depleted from the solution as they deposit onto the electrodes and the electrodes are removed from solution. Thus the chitosan solution decreases in concentration after every deposition. After a year, it is possible that after many depositions the concentration has dropped enough to affect concentration and thus the thickness of the films.

#### *4.6.2 Measurement and Analysis Error*

There is also significant error in the quantitative roughness measurements by AFM. Besides the fact that the films are not homogeneous over an electrode and that the sample size (i.e.  $2 \times 2 \mu\text{m}$ ) is a very small fraction of the overall surface area ( $1 \times 1 \text{ cm}$ ), roughness is also highly sensitive to tip history and sharpness. As a tip is scanned, it tends to pick up dust and dirt. While these particles are very small, they make a large difference when scanning at high resolution. The dirtier or less sharp the tip, the less sensitive the tip is to sharp and small features. The only way to really get accurate results is by using a

fresh tip with every scan or to do the entire procedure from deposition to analysis in a clean room. However, AFM tips are very expensive, they are not all precisely the same size, and they are time consuming to replace. Thankfully, general trends in roughness can be recognized if using a large enough sample size (number of scans or electrodes) and difference in deposition parameters for a large difference in roughness.

When examining AFM images, it is important to use the same parameters, like scan size, z height, flatten order, color contrast and offset. For surface images, also use the same rotation and pitch. This is because the images and interpretation of the images are highly sensitive to these parameters. Images can be tweaked to “say what you want them to say” by changing image processing parameters.

## Chapter 5: Results of Secondary Studies

Several other studies were performed parallel to the roughness and morphology study as a function of deposition parameters. The effect of neutralization on roughness, morphology, and chemistry was studied, along with spatial resolution, functionalization, and morphology of wet chitosan.

### 5.1 Effect of Neutralization on Roughness and Morphology

In deposition A, the effect of neutralization on roughness and morphology was examined. It has already been reported that neutralized films are thinner and more compact than they are before they were neutralized [12]. However, because of the apparent effect of the thickness on roughness, it is hard to know whether a reduction in roughness due to neutralization is due to a reduction in thickness or a change in the conformation and surface chemistry of the film.

There was not a reliable trend in the effect of neutralization on roughness. While the neutralized roughness values were in general less than the non-neutralized roughness values, this was found to be likely due to the difference in dimensions of the scan (this was before I discovered the importance of scan size). When comparing only scans of the same size (5 x 5  $\mu\text{m}$ ), it is possible to compare the neutralized and non-neutralized samples, but with a sample size so small and with differences within the error bars, the results are inconclusive. While neutralizing the films after deposition should theoretically reduce the roughness, neutralizing is likely to have little effect on films that have been already dried for two months.

## 5.2 Morphology of Wet Chitosan Films

While characterization of hydrated films is much more difficult, it provides important information about the properties of chitosan films *in situ*. Preliminary AFM results show that the surface morphology differs noticeably according to degree of hydration. Hydrated films, though thicker than when dry, are actually smoother. Rather than form rough ridges, the wet films have larger circular islands with rather smooth and flat plateaus as shown in Figure 17.

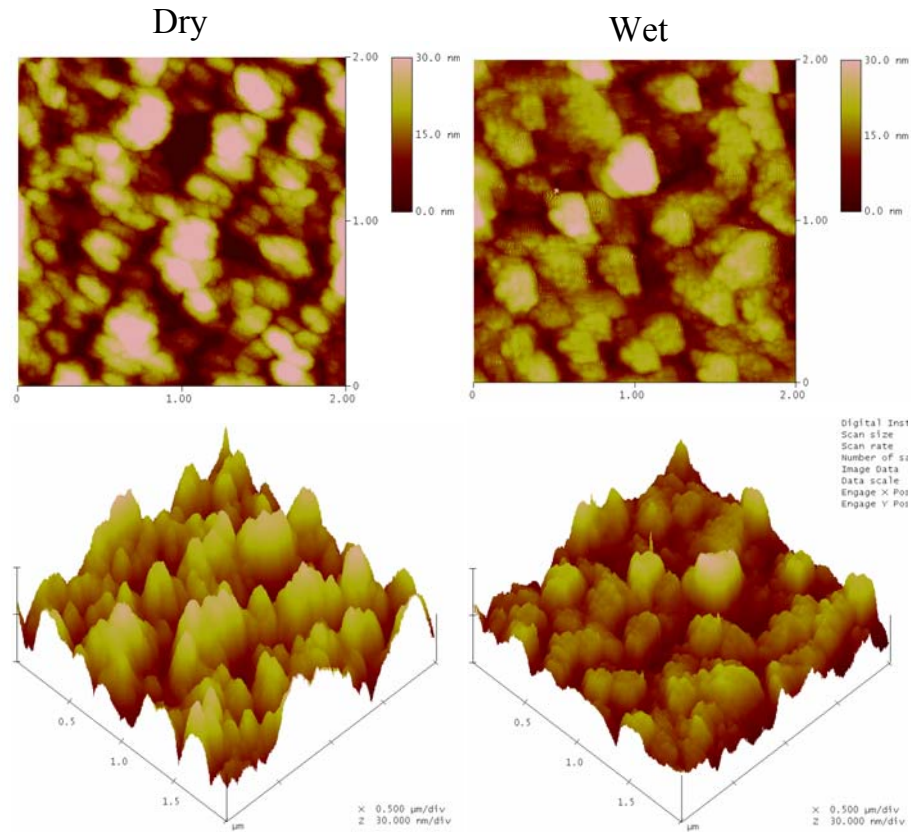


**Figure 17. Dry and wet chitosan films have different morphologies.**

This phenomenon is in agreement with the findings of Xiaolong Luo. Luo studied the surfaces of fluorescently-labeled, dried chitosan films using a stylus profiler, and fluorescence microscopy. Fluorescence microscopy maps the spatial distribution of

chitosan across the deposition electrode, enabling a comparison of in-vitro and dry morphology of the chitosan film. Luo measured the intensity of the fluorescence across the electrode surface using a program called Image-J. A comparison of a cross section of the fluorescent profile with the physical profile from the stylus profiler showed that a map of fluorescent intensity correlates with physical surface dimensions. Following these results, he measured the intensity of the fluorescence of wet films in solution. He found that these films were much smoother than their dry counterparts as shown in Figure 18, which is in agreement with the AFM images and roughness calculations. In conclusion, air-dried films are much rougher, indicating non-uniform and unpredictable collapse of the film's structure during drying.

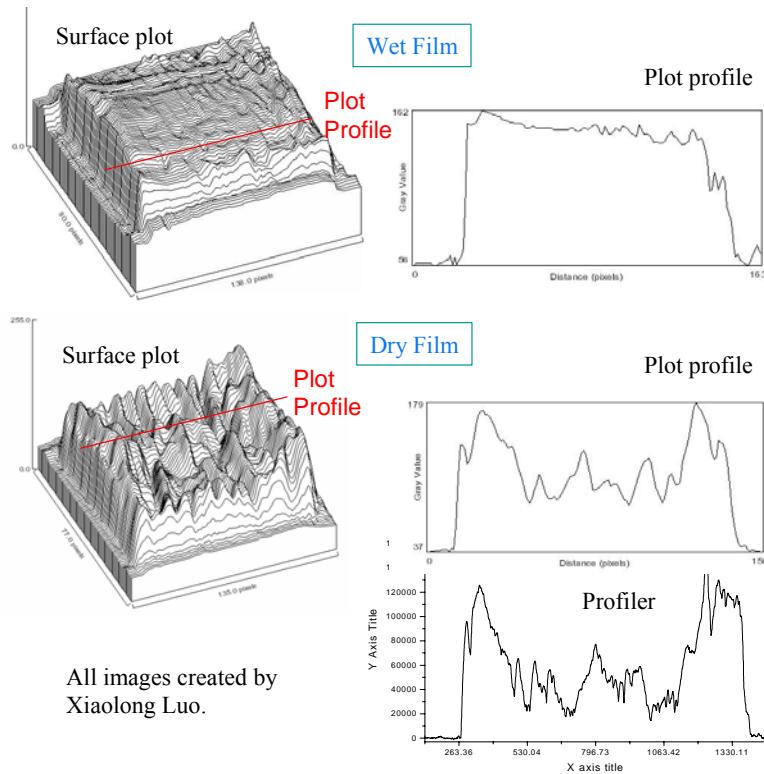


**Figure 18. Fluorescent intensity maps demonstrate that dry films are much rougher than wet ones.**

### 5.3 Using Raman Spectroscopy to Identify Functional Groups

Raman spectra were obtained for half of the films from deposition A before and after neutralization for determining chitosan's functionality and the effect of neutralization on it. Raman spectra were analyzed for fingerprint and group frequency peaks. Group frequency peaks tend to occur above  $1500\text{ cm}^{-1}$ , while fingerprint modes are unique to the specific molecule and are usually found below  $1500\text{ cm}^{-1}$  [13]. Before starting the analysis, the chemical structures of chitin and chitosan were examined for the groups they contained in order to know what to expect. The functional groups identified are presented in Table 9.

	<b>Group</b>	<b>Char. Freq. (<math>\text{cm}^{-1}</math>)</b>
<b>Chitosan</b>	Alkane: C-C, C-H (methylene)	2850-2960
	Amine: $\text{NH}_2$ (primary)	pair of peaks, 3350-3400 and 3270-3330
	Alcohol: C-OH	3600-3200
	Ether: C-O-C	1100
<b>Chitin</b>	Mono subst Amide: $\text{NH-C=O-CH}_3$	1260 (Amide III)
	Amine: NH (secondary)	3350-3310
	Methyl, $\text{CH}_3$ :	bend, 1460; def 1375

**Table 9. Raman excitation frequencies for functional groups present in chitosan and chitin. The groups listed for chitin are in addition to the groups contained in chitosan with the exception of the primary amine group.**

While obtaining the Raman spectra requires little skill, performing the analysis is no easy feat. When analyzing a spectrum, start at the high frequency end and concentrate on the very intense peaks first. In general, do not try to account for all the peaks because

most are usually fingerprint peaks anyway. Also, be aware of peaks that can be an overtone caused by resonance [13]. Aided by reference 13, the group frequencies were first assigned to the spectra. The most prominent peak occurs around  $2900\text{ cm}^{-1}$ . This peak is due to alkane vibrations.

### *5.3.1 Alkane Analysis*

Examining the molecules, chitosan contains 5 methine (C-H) groups per repeat unit and 1 methylene ( $\text{CH}_2$ ) group. Chitin contains 5 methine, 1 methylene, and 1 methyl group per repeat unit. According to source 13, methyl groups have a doublet at  $2962\text{ cm}^{-1}$  and  $2872\text{ cm}^{-1}$ , while methylene has a doublet at  $2926\text{ cm}^{-1}$  and  $2853\text{ cm}^{-1}$ . However, according to reference 14, a methylene stretching doublet occurs at  $2935 \pm 10\text{ cm}^{-1}$  due to asymmetrical stretching and  $2883 \pm 10\text{ cm}^{-1}$  due to symmetrical stretching. This is in fact seen in the chitosan spectra in Figure 19 with values around  $2883\text{ cm}^{-1}$  and  $2936\text{ cm}^{-1}$  observed. In addition, it is more likely that source 14 is correct for this application since chitosan is a biological material and is being analyzed using Raman rather than IR spectroscopy, which was the focus of that chapter in source 14. Moreover, according to source 13, methyl  $\text{CH}_3$  bending can be found at  $1460 \pm 10\text{ cm}^{-1}$  and  $\text{CH}_3$  deformation at  $1375 \pm 10\text{ cm}^{-1}$ . These peaks are present in Figure 20, indicating incomplete deacetylation.

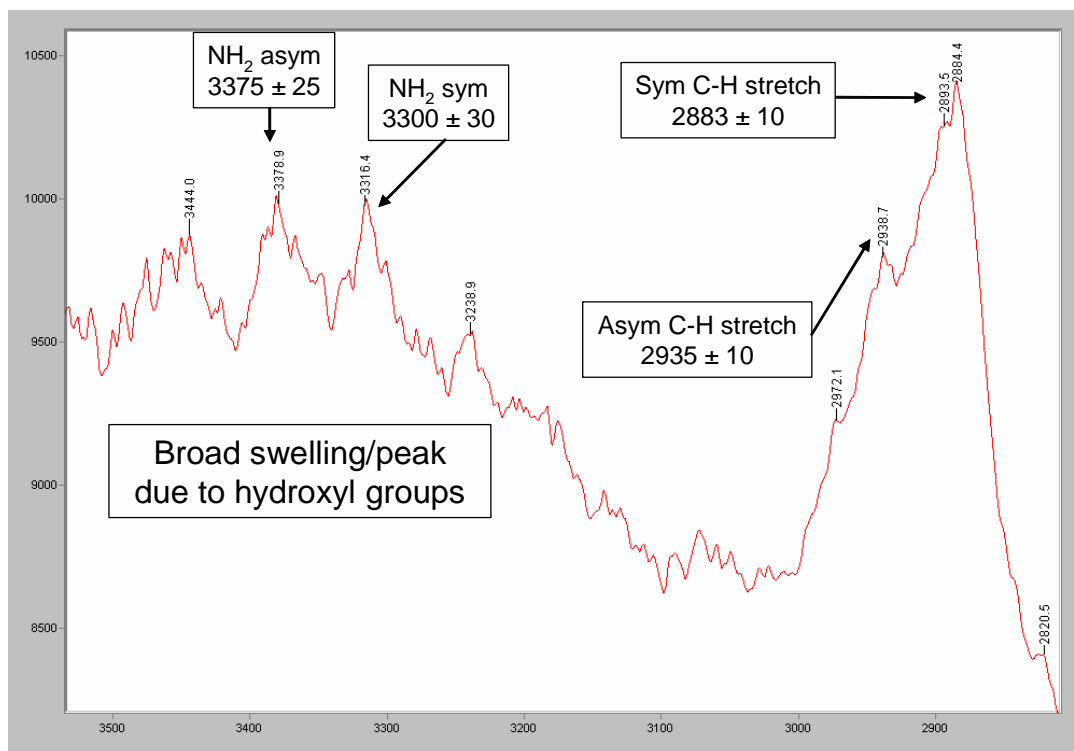


**Figure 19.** The high wavenumber end of the chitosan spectrum contains alkane, amine, and hydroxyl peaks.

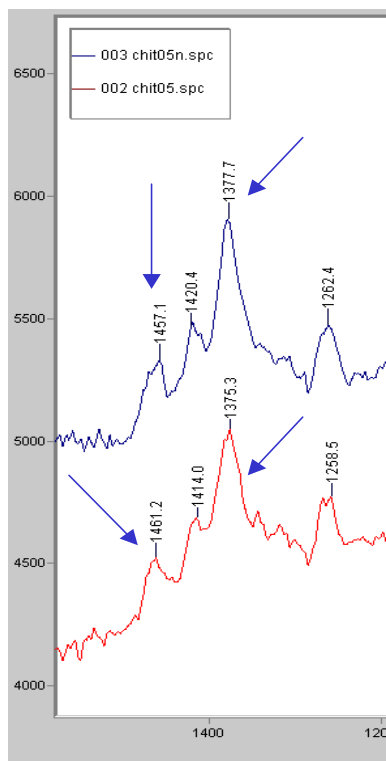


**Figure 20. Methyl peaks present in the chitosan spectrum indicate chitin.**

### 5.3.2 O-H and N-H Analysis

X-H systems occur at high frequencies and do not tend to interact with any other vibrations except for each other, making them highly diagnostic and reliable [13].

Unfortunately, both O-H and N-H are present in chitin and chitosan. Alcohols have different characteristic frequencies depending on the substitution of the carbon the O-H is attached to.  $\text{RH}_2\text{COH}$  is primary,  $\text{R}_2\text{HCOH}$  is secondary, and  $\text{R}_3\text{COH}$  is tertiary. Both chitosan and chitin have one primary and one secondary alcohol. Primary O-H has a peak at  $3640\text{ cm}^{-1}$  and secondary O-H has one at  $3630\text{ cm}^{-1}$  [13]. However, in Raman, all O-H bands are very weak, causing a very broad peak or swell as shown in Figure 19. IR

spectroscopy would need to be executed to examine these groups as O-H is stronger than N-H in IR. Thankfully, the reverse is true for Raman.

Raman spectroscopy is very helpful for distinguishing amines from alcohols because the N-H stretch is distinctly stronger than is the O-H stretch [13]. Also, hydrogen bonding has less of an effect on amines than alcohols, which changes the spectra completely. There is one primary amine in the chitosan repeat unit. Aliphatic (refers to alkanes versus aromatic which refers to benzene rings) primary amines have peaks at  $3375 \pm 25 \text{ cm}^{-1}$  (out of phase or asymmetric stretch) and  $3300 \pm 30 \text{ cm}^{-1}$  (in phase or symmetric stretch). These peaks are seen as shown in Figure 18. Chitosan spectra did not show  $\text{NH}_2$  scissoring at  $1620 \text{ cm}^{-1}$  or  $\text{NH}_2$  wagging at  $800 \text{ cm}^{-1}$ . However, it is common for peaks to be missing so there is no cause for alarm. There is also a secondary amine in the chitin repeat unit. The secondary NH stretch occurs at  $3300 \text{ cm}^{-1}$ . This is likely overlapping with the primary amine peak at the same frequency so it will be hard to distinguish between the two. The NH bend occurs at  $1500 \text{ cm}^{-1}$ , but it also is not seen.

### *5.3.3 Amide and Ether Analysis*

Chitin contains one secondary amide per repeat unit. This gives an N-H stretch at  $3300 \pm 20 \text{ cm}^{-1}$ , as well as amide I at  $1650\text{-}1640 \text{ cm}^{-1}$ , amide II from  $1570\text{-}1530 \text{ cm}^{-1}$ , and amide III in  $1300\text{-}1220 \text{ cm}^{-1}$ . However, these peaks are strong or very strong in IR which means that they are not in Raman. Source 13 adds that the amide III may be seen in Raman better than IR, but is the only exception. Consequently, the  $\sim 1260 \text{ cm}^{-1}$  peak could be amide III. However, source 14 says that amide I and amide II are found in Raman, but amide III is not. Thus this assignment of the  $\sim 1260 \text{ cm}^{-1}$  peak is tentative. Otherwise, no signs of an amide are present in the spectra.

Saturated ethers have a peak at  $1100 \pm 50 \text{ cm}^{-1}$ . This peak is present in the spectra, though source 13 says it is unimpressive in Raman. Three peaks are seen in this region. A maximum middle peak occurs around  $1115 \text{ cm}^{-1}$ . A slightly shorter or about the same height peak occurs just to the right at about  $1100 \text{ cm}^{-1}$ . A smaller shoulder to the left occurs around  $1150 \text{ cm}^{-1}$ . There is no explanation other than fingerprint for the multiple peaks. These peaks are shown in Figure 21.

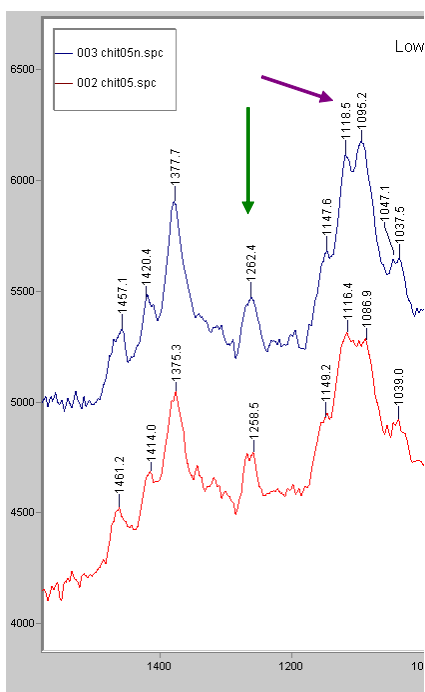


**Figure 21. Amide (green) and ether (purple) peaks in the chitosan spectrum.**

#### 5.3.4 Effect of Neutralization on Amine Peak Intensities

Before neutralization, there should be residual ammonium groups,  $\text{NH}_3^+$ . This should show a difference between the before and after neutralization spectra. In an  $\text{NH}_3^+$  salt, the band due to stretching will be much lower than in  $\text{NH}_2$ . There will often be several bands in the  $2800\text{-}2200 \text{ cm}^{-1}$  region, sometimes weak, sometimes strong [13]. However, no peaks are observed in this region at all. None of the spectra show evidence

of amine salts. ITC-irst results by XPS showed  $<0.5\%$  of the groups were  $\text{NH}_3^+$ .

Assuming that the same is true here, the concentration of ammonium is too small for Raman to detect and thus the absence of the peaks is expected.

Comparing the amine group intensities before and after neutralization, the peaks seem to intensify slightly after neutralization as shown in Figure 22. This could indicate that a few groups changed from  $\text{NH}_3^+$  to  $\text{NH}_2$ , but that the  $\text{NH}_3^+$  groups were not concentrated enough to produce bands in the spectrum. However, the slight increase in intensity could also be due to error during Raman analysis. The intensities should be properly normalized by a peak that shouldn't change with neutralization and then compared.

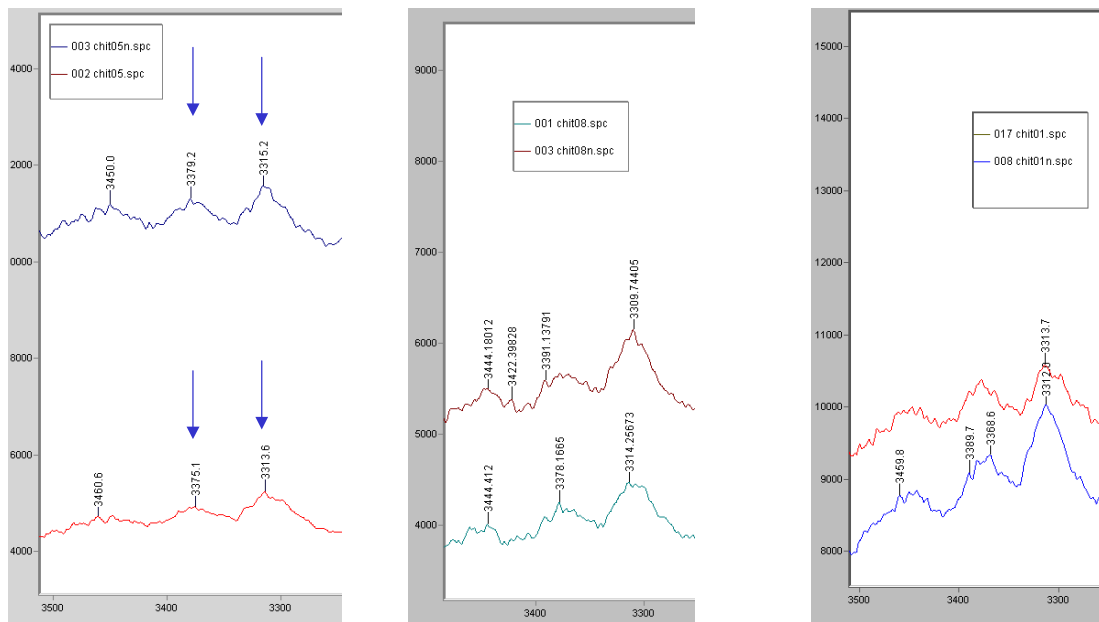


**Figure 22. The intensity of amine peaks increases after neutralization.**

#### 5.4 Determination of Spatial Resolution using Raman Spectroscopy

Spatial selectivity of chitosan deposition is important for further miniaturization of patterns for smaller devices. Previously, we selectively deposited both fluorescently

labeled chitosan and chitosan that was later reacted with NHS-fluorescein onto negative micropatterned gold electrodes. Using fluorescence imaging, we showed spatial selectivity of chitosan down to 20  $\mu\text{m}$  by using a wide range of pattern thicknesses and separations [10]. On the currently used chips, residues surrounding the gold electrodes were observed. Optically, it was unclear whether the residues were chitosan or residual salts that deposited during neutralization, rinsing, and drying steps. It was also not obvious through the study of surface roughness and morphology with AFM. Therefore, Raman microspectroscopy was implemented to chemically investigate the identity of the residues. Exploring the identity of the residues also provides information about the spatial selectivity of the electrodeposition process. Rather than reduce the size of the patterns and proceed as described previously, spatial resolution below 20  $\mu\text{m}$  can be studied simultaneously.

The expected Raman spectrum was obtained as described in Section 2.2.3 and 5.3, and is pictured in Figure 23a. It is possible to identify within 1  $\mu\text{m}$ , the diameter of the laser spot, where chitosan is and is not present based on its unique spectrum. However, chitosan less than 100 nm thick cannot be detected with this technique as shown in Figure 22b. The thickest sample, 3, with a thickness of 875 nm, has the most intense signal. Intensity decreases for sample 2 of thickness 433 nm. The 10 nm and 85 nm (not shown) films yield no signal above the noise level. Signal strength or intensity is dependent on film thickness because the sampling depth is 2  $\mu\text{m}$ , thicker than the chitosan films. Thus a reduction in thickness reduces the number of scattering centers reducing the intensity of the peaks. Therefore amine site density, a useful parameter for biological reactions, cannot be determined using this technique without normalizing the thickness.

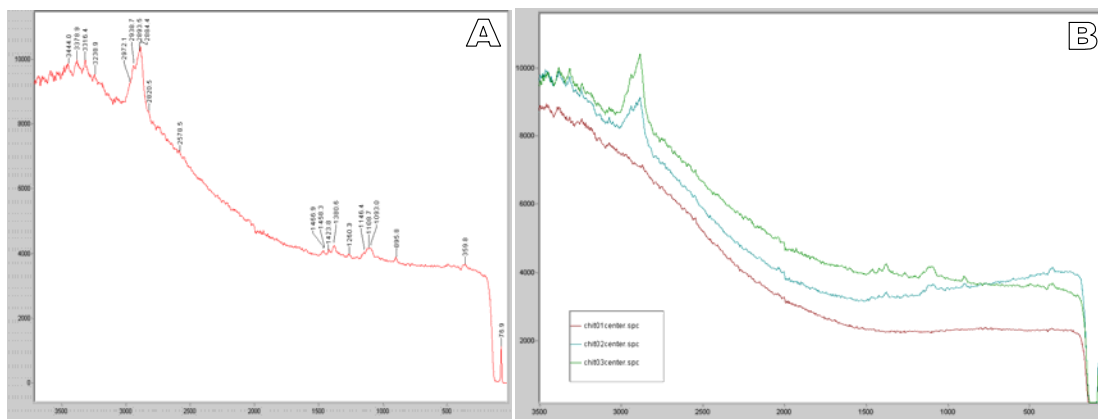


**Figure 23. Full Raman spectra of chitosan. A: Typical spectrum with peak values. B: Peak intensity increases with film thickness.**

Raman spectra were obtained near the electrodes to determine the chemical identity of the residues. The spectra taken just off the edge of the gold were then compared with typical spectra from the center of the chitosan covered gold electrode and from the substrate (“silicon”) far from the electrode. As shown in Figure 24, the laser, indicated by the red circle, samples an area with a 1  $\mu\text{m}$  diameter 1-3  $\mu\text{m}$  from the Au pad. These spectra near the gold (“edge”, “outedge”) did not have a chitosan signature; chitosan was identified on the border of the gold to show that Raman does indeed identify chitosan correctly when present. The substrate spectrum is identical to the one taken on the residue by the edge.

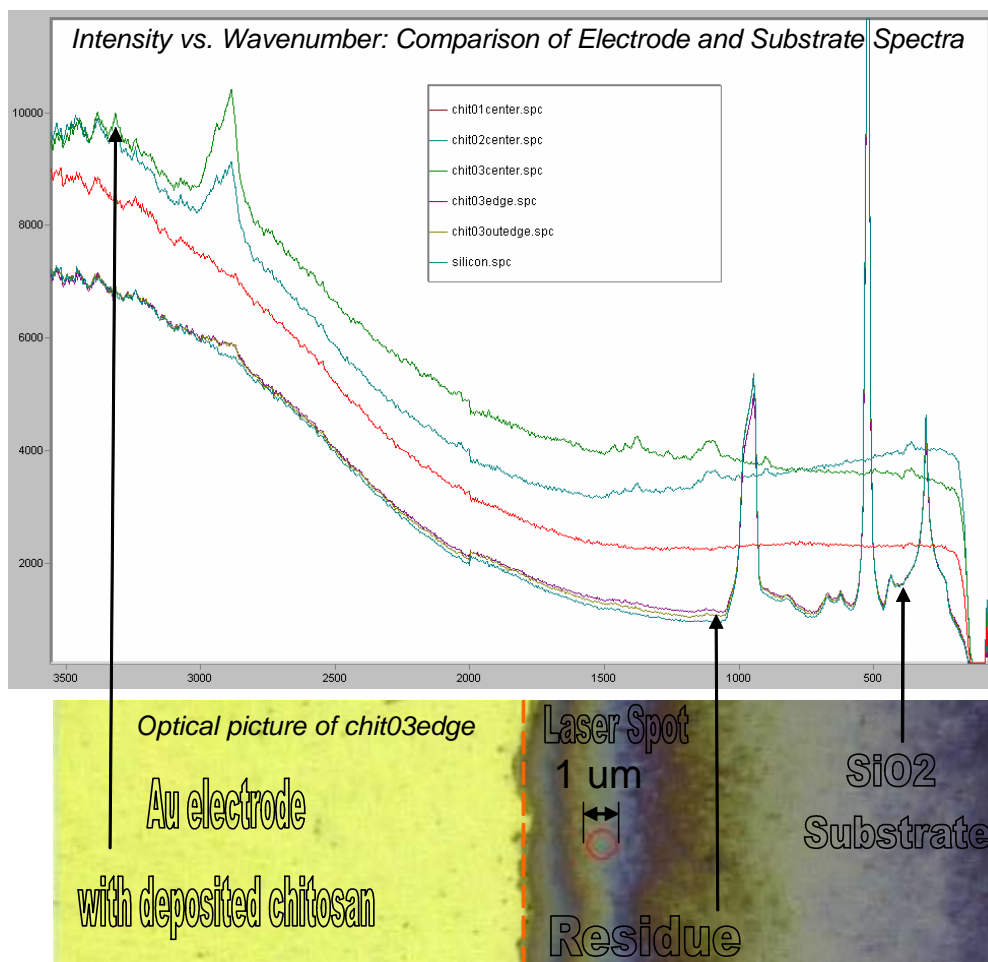


**Figure 24. Spatially selective Raman spectra show residues on substrate are not chitosan.**

Results show that spatial resolution is on the order of 1-2  $\mu\text{m}$ , but they are not completely conclusive. For example, there could be residues on the substrate that do not appear optically, but are Raman active. Another possibility is that the residue is not Raman active so that only the  $\text{SiO}_2$  spectrum appears with or without residue. This is more likely since the residue is thick enough to produce a measurable signal assuming it is Raman active. Furthermore, it is possible that a very small number of chitosan molecules extend past the edges of the gold, but that they are so thin or sparse that Raman microspectroscopy cannot detect them. Further experimentation with adequate controls is

needed for complete certainty about the spatial resolution and the identity of the substrate peak and/or residues.

## Chapter 6: Conclusions

### 6.1 Summary of Conclusions

Chitosan is an extremely complex and difficult molecule to work with. It is hard to predict and reproduce its behavior. The growth of amorphous chitosan films is non-linear for both the thickness and the roughness. For dry films, atomic force microscopy revealed that the roughness scales with the thickness logarithmically, at least for thin films and up to the hydrogel range. The trend in the hydrogel range is not wholly conclusive, but it appears that roughness increases rapidly in this range, creating an s-shape curve over a large range of thicknesses. This data supports a nucleation or run away model where the first chitosan molecules are attracted to defects in the gold electrode and subsequent molecules are then further attracted to the now larger defects. Eventually the defects grow into each other and the growth of the film's roughness begins to slow and level off.

In summary:

- For same scan size and current density, as time increases:
  - thickness increases
  - roughness increases
  - the film becomes more heterogeneous
- Wet films are thicker, smoother and have a different morphology than their dry counterparts
- Spatial resolution, at least after the chitosan dries, is within 2  $\mu\text{m}$  as confirmed by Raman microspectroscopy

Smaller lessons were also learned throughout the process. The first was that AFM scan size has a huge effect on the roughness. When comparing roughness values, data must be obtained from the same scan sizes. When processing, the same flattening order must be used for all samples since this affects the roughness as well. The industry standard is for flattening to be done before roughness analysis. In Raman microspectroscopy, the intensity of the signal is affected by thickness when less than 2  $\mu\text{m}$  of film is grown.

## 6.2 Future Work

Following the results and conclusions of this study, further research could be carried out in several directions. One interesting study would be to measure the density of the films as a function of current density. Density could be qualitatively measured using SEM to look at the surface structure and cross section. Theoretically, higher current densities produce lower density films. Lower density means that the film is more porous and has more surface area. More surface area is beneficial for greater attachment of biomolecules. In addition, the porosity could be tailored for different applications.

Moreover, the roughness values calculated in this study were average roughnesses which do not account for the frequency of peaks, the periodicity. Power Spectral Density (PSD) analysis could be used to account for this. PSD information would probably be more useful and would give a more complete picture of the surface of these films, but it is very complex and much less user friendly.

To test the theory of defect nucleated growth, defects could be templated into the gold in a regularly ordered fashion [15]. Films could be grown for short periods of time and the surface observed using AFM. If the films have an ordered structure

corresponding with the structure of the template, then the theory would be supported. If the films looked no different, then the theory would not be proven and another method would need to be developed to study the growth.

It would be especially interesting and useful to study the surface morphology of wet films in solution in the AFM. The effect of pH and ion concentration could be studied in addition to the effect of deposition parameters. This method most accurately reflects real life since the films are used primarily in solution. Another interesting study would be to look at the effect of relative humidity on the swelling or thickness and surface roughness of chitosan. We already know that chitosan swells in water and shrinks when dehydrated, and reswells again in water. It would be interesting to know how fast and how effectively it reswells with repetition.

Raman spectroscopy was initially chosen as a mode for chemical structure identification. However, further expertise is needed in order to use Raman spectroscopy to determine structural aspects of the films. Identification of chemical groups is not too difficult, but structural determination requires lots of time and careful analysis as well as experience and expertise. With this, Raman could be used for calculating amine site density, and the effect of different neutralizing agents and ion concentration on structure. These could also be performed in solution if the proper objectives are ordered. Then many exciting scientific experiments could be executed.

## REFERENCES

1. Rubloff, Gary. Private communications. 2005.
2. X:\labs\cacse\gwr-group\res\_biomems\experimental\materials\chitosan  
    \BLURBsonChitosan.doc
3. “Structure of Chitin/Chitosan and Cellulose.” 12 Apr. 2002. *Dalwoo BLS*. 27 Apr. 2005 <<http://dalwoo.com/chitosan/structure.htm>>.
4. “Dimension 3100 Datasheet” 2006. Veeco Instruments. 20 Apr. 2005.  
    <[http://www.veeco.com/html/datasheet\\_d3100.asp](http://www.veeco.com/html/datasheet_d3100.asp)>.
5. D.W. Mayo, F.A. Miller, and R.W. Hannah. *Course Notes on the Interpretation of Infrared and Raman Spectroscopy*. Hoboken, NJ: Wiley Interscience, 2004.
6. H. Gremlich and B. Yan. *Infrared and Raman Spectroscopy of Biological Materials*. NY: Marcel Dekker, 2001.
7. Pedroni et al., *Colloid Polymer Science*, **282**, 100–102, (2003).
8. Ottoy et al., *Carbohydrate Polymers*, **29**, 17-24, (1996).
9. Aiba et al., *International Journal of Biological Macromolecules*, **13**, 40-44, (1991).
10. Kurita et al., *Makromol. Chem.*, **178**, 3197-3202, (1977).
11. L. Wu et. al., *Langmuir*, **19**, 519-524, (2003).
12. R. Fernandes et. al., *Langmuir*, **19**, 4058-4062, (2003).
13. Ghandehari, Hamid. Private communication. 10 Jan. 2006.
14. L. Wu et. al. *Langmuir*, **18**, 8620-8625, (2002).
15. Perez, Israel. Private communication. 3 Mar. 2006.